Molecular Therapy
Oncolytics
Original Article

oHSV2 Can Target Murine Colon Carcinoma by Altering the Immune Status of the Tumor Microenvironment and Inducing Antitumor Immunity

Wen Zhang,[1,6] Xiao Hu,[2,6] Jing Liang,[3] Yujie Zhu,[2] Beibei Zeng,[3] Lin Feng,[2] Changyun Zhao,[5] Shangmei Liu,[3] Binlei Liu,[4] and Kaitai Zhang[2]

[1]Department of Immunology, National Cancer Center/National Clinical Research Center for Cancer/Cancer Hospital, Chinese Academy of Medical Sciences and Peking Union Medical College, Beijing 100021, China; [2]State Key Laboratory of Molecular Oncology, Department of Etiology and Carcinogenesis, National Cancer Center/National Clinical Research Center for Cancer/Cancer Hospital, Chinese Academy of Medical Sciences and Peking Union Medical College, Beijing 100021, China; [3]Department of Pathology, National Cancer Center/National Clinical Research Center for Cancer/Cancer Hospital, Chinese Academy of Medical Sciences and Peking Union Medical College, Beijing 100021, China; [4]Hubei University of Technology, Nanhu, Wuchang District, Wuhan 430068, China; [5]Chongqing Deepexam Bioltechnology Co., Ltd., Chongqing 400020, China

Oncolytic viruses are promising immunoreagents. Numerous studies have shown that oncolytic virotherapy is effective for many tumors. Herein, we investigated the therapeutic effect of oHSV2, an oncolytic type 2 herpes simplex virus, on mouse colon carcinoma. The *in vivo* antitumor efficacy of oHSV2 was observed in both unilateral and bilateral colon cancer models. oHSV2 effectively eliminated tumors and prolonged the survival of mice without side effects. Additionally, treatment with oHSV2 effectively prevented the growth of rechallenged tumors and distant implanted tumors. The specific killing ability of splenic immune cells to tumor cells was enhanced. oHSV2 treatment effectively reduced the content of inhibitory immune cells (regulatory T cells [Tregs] and myeloid-derived suppressor cells [MDSCs]) and increased the content of positive immune cells (natural killer [NK], $CD8^+$ T, and dendritic cells [DCs]) in the spleen. Moreover, treatment with oHSV2 remodeled the tumor immune microenvironment. In summary, treatment with oHSV2 can effectively eliminate primary tumors, generate tumor-specific immunity, and elicit immune memory to inhibit tumor recurrence and metastasis. Furthermore, this virotherapy can reshape the immune status of the spleen and tumor microenvironment in mice, which can further improve the therapeutic antitumor effect.

INTRODUCTION

Colorectal cancer ranks third in incidence (10.2%) and second in mortality (9.2%) worldwide.[1] Recently, the combination of multiple drugs, the optimization of surgical approaches, and the gradually improved accuracy of radiotherapy target delineation have led to rapid progression of traditional treatment methods. However, conventional treatment has a limited therapeutic effect. Nearly half of all colorectal cancer patients present with metastasis at diagnosis or recurrence after a certain period of treatment and have a low 5-year survival rate.[2] As the understanding of tumor immunity and immune escape mechanisms has been enhanced, new and more effective tumor immunotherapies have emerged. Methods to break the immune tolerance of the tumor microenvironment (TME) effectively prevent tumor immune escape and more potently stimulate antitumor immunity in the body without stimulating or even suppressing negative immune responses are novel approaches for the design of new therapeutic modalities. For the past few years, the emergence of virotherapy and in-depth research into it has shed new light on the treatment of solid tumors.[3] Oncolytic viruses (OVs) have attracted much attention because of their unique characteristics.

Oncolytic virotherapy is a potential biotherapy that uses wild-type and engineered viruses to treat malignancies. Viruses can be designed to selectively recognize, infect, and destroy malignant cells with minimal effects on normal human cells. Malignant cells can be killed directly by an overwhelming viral infection, which releases additional viral particles to infect neighboring cells.[4] Viral infections also activate the immune system.[5] Increasing evidence has shown that OVs stimulate a series of antitumor immune responses, leading to immunogenicity in the TME and regulation of the immunosuppressive TME.[6] Tumor cell lysis results in the release of tumor-associated

Received 15 August 2019; accepted 24 December 2019;
https://doi.org/10.1016/j.omto.2019.12.012.

[6]These authors have contributed equally to this work

Correspondence: Kaitai Zhang, State Key Laboratory of Molecular Oncology, Department of Etiology and Carcinogenesis, National Cancer Center/National Clinical Research Center for Cancer/Cancer Hospital, Chinese Academy of Medical Sciences and Peking Union Medical College, Beijing 100021, China.
E-mail: zhangkt@cicams.ac.cn
Correspondence: Binlei Liu, Hubei University of Technology, Nanhu, Wuchang District, Wuhan 430068, China.
E-mail: 1836035949@qq.com
Correspondence: Shangmei Liu, Department of Pathology, National Cancer Center/National Clinical Research Center for Cancer/Cancer Hospital, Chinese Academy of Medical Sciences and Peking Union Medical College, Beijing 100021, China.
E-mail: liu_shangmei@sina.com

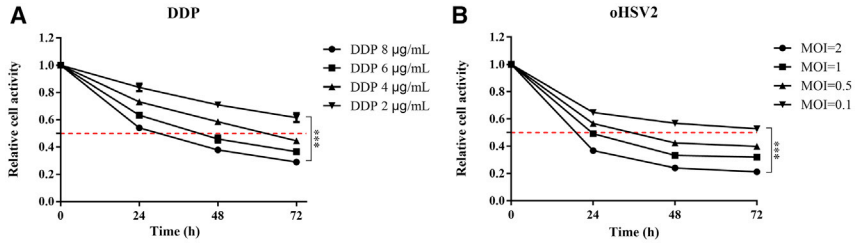

Figure 1. CCK-8-Based Cell Viability Assay Revealing the Effect of DDP and oHSV2 on CT26 Cell Viability *In Vitro*

(A) CT26 cells were treated with DDP at different concentrations (2, 4, 6, and 8 μg/mL) for 24, 48, and 72 h. $p < 0.001$. (B) CT26 cells were infected with oHSV2 at different MOIs (0.1, 0.5, 1, and 2) for 24, 48, and 72 h. $p < 0.001$.

antigens (TAAs) and simultaneous expression of pathogen-associated molecular patterns (PAMPs) and danger-associated molecular patterns (DAMPs), which stimulate innate immune receptors on professional antigen-presenting cells (APCs).[7,8]

OVs can promote the antitumor T cell response through various mechanisms. For example, they trigger immunogenic cell death in tumor beds, which can promote the maturation and function of dendritic cells (DCs).[9] Stimulated DCs produce large amounts of type I interferons (IFNs) and pro-inflammatory chemokines and cytokines, which further induce widespread pro-inflammatory effects, leading to the recruitment of T cells and the regulation of immune responses.[10] This process facilitates the destruction of the physical barrier that inhibits T cell infiltration.[11] Recruitment of immune cells triggers immune checkpoints that limit the expansion of the inflammatory response. OV therapy can heat up immunologically "cold" tumors by enabling immune checkpoint blockade and converting immunosuppressive cells to a pro-inflammatory phenotype to effectively break the immune tolerance of the TME.[12] In addition, OVs can improve the immune system recognition of tumor cells by upregulating the process of antigen processing and presentation. In response to the action of APCs, TAA-specific central memory T cells accumulate in the splenic follicles, resulting in antitumor T cell responses.[13] Therefore, OVs have the potential to eliminate primary, recurrent, and metastatic tumors.[4]

In this study, we used an oncolytic herpes simplex virus type 2 (oHSV2) with deletions in the ICP34.5 and ICP47 genes. The specific procedure used to construct this virus has been described previously.[14] In addition, our previous studies showed that oHSV2 can infect most human and mouse tumor cell lines and exhibits strong oncolytic activity. oHSV2 also exhibited significant antitumor activity and safety in a 4T1 tumor animal model.[14] In this study, we evaluated the antitumor effect of oHSV2 in CT26 tumor animal models and observed its effect on recurrent and metastatic tumors. By further investigating the changes in the tumor immune microenvironment, we demonstrated that oHSV2 therapy induced a specific antitumor immune response and had a long-term effect.

RESULTS

Both oHSV2 and Cisplatin Effectively Reduce the Viability of CT26 Cells

A Cell Counting Kit-8 (CCK-8) proliferation assay was performed with cells treated with oHSV2 and cisplatin (DDP). To estimate the effects of oHSV2 and DDP, CT26 cells were incubated with different multiplicities of infection (MOIs) of oHSV2 (0.1, 0.5, 1, and 2) and different concentrations (2, 4, 6, and 8 μg/mL) of DDP. CT26 cells were sensitive to oHSV2 and DDP, and cell viability decreased in a time- and dose-dependent manner (Figure 1). For MOIs equal to or greater than 1, cell viability was reduced by 50% or more 24 h after viral infection (Figure 1B).

oHSV2 Treatment Inhibits Tumor Growth and Prolongs Survival

The therapeutic effects of oHSV2 and DDP were further examined *in vivo* (Figure 2A). During the treatment and observation period, tumors in the mock group exhibited central necrosis or cavitation when the size increased to 600–1,000 mm^3. Tumors in the oHSV2 treatment group exhibited necrosis in the early stages of treatment at a size of 100–200 mm^3, and a local black scab and tumor regression appeared. On day 13 after the first treatment, one mouse in the oHSV2 treatment group exhibited tumor regression. Subsequently, the number of mice with tumor regression in this group gradually increased. No tumor regression was observed in the mock group, indicating that effective tumor necrosis occurred in the advanced stage in the mock group due to the large tumor size and nutrient deficiency. Tumor necrosis occurring in the early stage after treatment with oHSV2 is probably caused by direct lytic killing of cancer cells.

On day 20 after the first treatment, the average tumor volume in the mock group was 1,998.830 ± 52.770 mm^3, while the average tumor volumes in the group treated with oHSV2 alone and the chemotherapeutic drug DDP alone were 16.493 ± 4.291 mm^3 and 868.944 ± 52.145 mm^3, respectively. Six mice in the OV treatment group were completely tumor-free. The average tumor volume after treatment with oHSV2 or DDP significantly differed compared with that in the mock group (****$p < 0.0001$, **$p = 0.0012$); the difference between the average tumor volume in the oHSV2 treatment group and that in the DDP treatment group was also significant (***$p = 0.0003$) (Figure 2B).

The mean weights of the mice in the mock, oHSV2, and DDP groups were 19.975 ± 0.112 g, 18.488 ± 0.222 g, and 14.650 ± 0.215 g, respectively, on day 12 after the first treatment. No significant differences (ns, $p = 0.6065$) were observed between the mock group and the oHSV2 treatment group, but significant differences were found between the DDP treatment group and both the mock group (**$p = 0.0013$) and the oHSV2 treatment

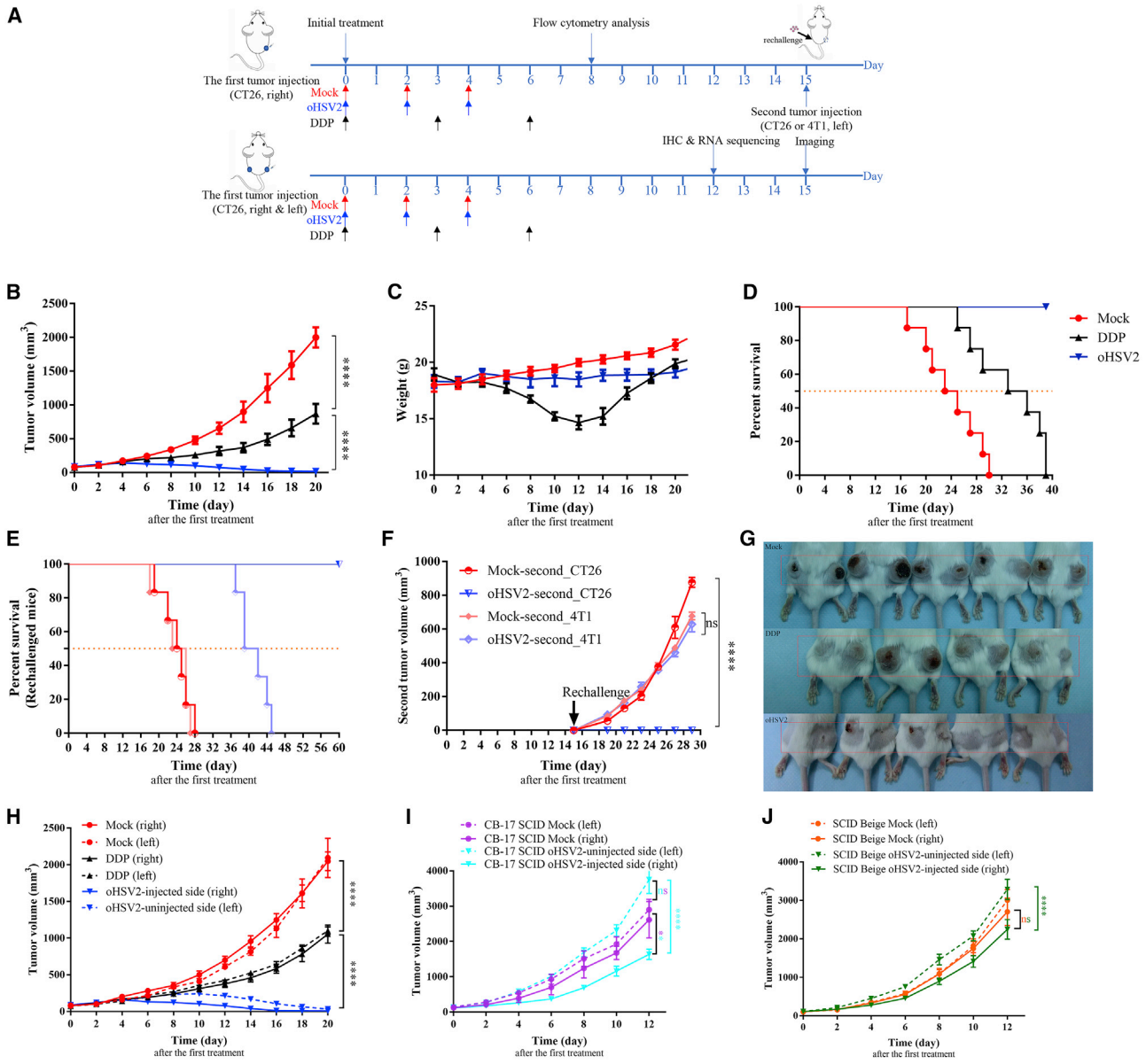

Figure 2. oHSV2 Treatment Inhibits Tumor Growth and Induces Systemic Immunity

(A) Timeline of tumor injection and treatment. At each time point, only the right-side tumor was treated. (B) Tumor growth curves for the three groups (mock, DDP, and oHSV2). Data are shown as the mean ± SEM; n = 8 mice/group. (C) Trends in mouse weight by day in the three groups. Data are shown as the mean ± SEM; n = 8 mice/group. (D) Kaplan-Meier survival analysis of the three groups (n = 8 mice/group). When the tumor volume reached 2,500 mm^3 or the mouse died naturally, the mouse was considered dead. (E) Kaplan-Meier survival analysis of the rechallenged mouse groups (n = 6 mice/group). When the volume of the tumor on either side reached 2,500 mm^3 or the mouse died naturally, the mouse was considered dead. (F) Growth curve for the second tumor after rechallenge with CT26 cells (3×10^5) or 4T1 cells (5×10^4) in the flanks of the cured animals at 15 days after the first treatment. Data are shown as the mean ± SEM; n = 6 mice/group. (G) The appearance of bilateral tumors following s.c. inoculation on day 15 after the first treatment. From top to bottom: mock, DDP, oHSV2. (H) Bilateral tumor growth curves for the three groups (mock, DDP, and oHSV2). Data are shown as the mean ± SEM; n = 5 mice/group. (I) Bilateral tumor growth curves for CB-17 SCID mouse model (mock and oHSV2 groups). Data are shown as the mean ± SEM; n = 6 mice/group. (J) Bilateral tumor growth curves for the SCID-beige mouse model (mock and oHSV2 groups). Data are shown as the mean ± SEM; n = 6 mice/group.

group (*p = 0.0171) (Figure 2C). Moreover, treatment with oHSV2 was associated with a very favorable mental profile. The behavioral activity and hair luster were unchanged. Mice in the DDP treatment group, in contrast, were listless, and their hair lacked luster (Figure S1). During the second half of the measurement period, the weight of the mice in the DDP group gradually increased, possibly because the effects of the chemotherapeutic drugs gradually diminished (Figure 2C).

When the tumor volume reached 2,500 mm^3 or the mouse died naturally, the mouse was considered dead. The data shown in Figure 2D suggest the superiority of oHSV2 over mock (34.5 days; ****p < 0.0001) and DDP (24 days; ****p < 0.0001) treatment in the median overall survival (OS). No deaths occurred in the oHSV2 treatment group during the observation period (Figure 2D).

Therefore, the conclusion can be made that treatment with either oHSV2 or the chemotherapeutic drug DDP inhibits the growth of CT26 tumors and improves the OS relative to mock treatment. Due to the lack of body weight loss and mental deterioration, the effect of oHSV2 was better than that of DDP.

oHSV2 Treatment Induces Systemic Antitumor Immunity

We next examined whether oHSV2 played a functional role in the overall immunity of mice and whether the immune response was tumor-specific. Fifteen days after the first treatment, six mice per group (mock and oHSV2) received another injection of CT26 or 4T1 tumor cells on the contralateral side of the body. Mice in the oHSV2 group inoculated with CT26 cells did not develop tumors and remained tumor-free and alive until the end of the observation period (60 days) (Figure 2E). However, the other mice in the oHSV2 group that were inoculated with 4T1 cells, as well as all mice in the mock group, exhibited significant ($p < 0.01$) tumor formation within 4 days after the second cell inoculation on the contralateral (left) side (Figures 2E and 2F). We repeated the experiment with intervals of 4 and 8 weeks before rechallenge of the cured mice and obtained similar results (Figure S2). These results show that oHSV2 treatment can lead to long-term immunity and immunological memory. Even more notably, the immune response is tumor-specific.

The animal model established by bilateral subcutaneous (s.c.). inoculation of CT26 cells into immunocompetent BALB/c female mice showed that unilateral (right-side) treatment with oHSV2 alone not only inhibited the growth of the right-side tumors (oHSV2-injected side) but also resulted in smaller tumors on the left side (oHSV2-uninjected side) than did mock treatment. These results demonstrate that treatment with oHSV2 can induce a systemic immune response (Figures 2G and 2H).

Adaptive Immunity Is Essential for the Antitumor Efficacy of Virotherapy

To identify the immune cells that are important in the antitumoral effect mediated by oHSV2 treatment, we conducted experiments in which CT26 bilateral tumor models were established with female CB-17 severe combined immunodeficiency (SCID) (T cell and B cell dysfunction) and SCID-beige (T cell, B cell, and natural killer [NK] cell dysfunction) mice. After the tumors were palpable, the right-side tumor in each mouse was treated with oHSV2 or with RPMI 1640 serum-free medium (SFM) as a control; the contralateral (left-side) tumor was left untreated. oHSV2 only partially inhibited the growth of virus-treated tumors. In the CB-17 SCID mouse (T cell and B cell dysfunction) model, the average volume of oHSV2-injected tumors was significantly less than that of oHSV2-uninjected tumors (****p < 0.0001) and mock-treated tumors (**p = 0.0036). However, the volumes of the oHSV2-uninjected tumors and mock group tumors did not differ significantly (ns, p = 0.3304) (Figure 2I). Similarly, in the SCID-beige mouse (T cell, B cell, and NK cell dysfunction) model, the average volume of oHSV2-injected tumors was significantly less than that of oHSV2-uninjected tumors (****p < 0.0001). However, the average volumes of oHSV2-injected tumors and mock group tumors did not differ significantly (ns, p = 0.2039) (Figure 2J).

In the context of adaptive immunity deficiency, oHSV2 treatment resulted in a delay in oHSV2-injected tumor growth, although the tumor on the untreated side grew rapidly. The presence of NK cells appeared to delay the growth of tumors on the treated side to a certain extent. Comparing the therapeutic effect in immunocompetent mice with that in immunodeficient mice revealed that adaptive immunity is essential for the antitumor efficacy of virotherapy.

oHSV2 Treatment Improves the Specific Response of Cytotoxic T Lymphocytes (CTLs) in the Spleen

To determine whether oHSV2 induced an enhanced tumor-specific CTL response, the spleen lymphocytes harvested from three groups were cultured with CT26 cells and 4T1 cells *in vitro* at effector cell/target cell (E:T) ratios of 100:1, 50:1, and 25:1. Lymphocytes from the oHSV2 group led to a significantly higher percentage of propidium iodide (PI)-positive CFSE-labeled CT26 cells, which showed a highly specific CTL response against CT26 cells but not against 4T1 cells (Figure 3; Figure S3). No specific CTL response was detected in lymphocytes from mouse spleens treated with DDP (Figure 3; Figure S3).

Application of oHSV2 Enhances Positive Immunity in the Mouse Spleen

The phenotype of immune cells in the spleen is an indicator of the condition of peripheral immunity in mice. We analyzed the percentages of different immune cells in the spleen using flow cytometry. Regulatory T cells (Tregs) and myeloid-derived suppressor cells (MDSCs) are two types of immunosuppressive cells. Following a 4-day rest after the final oHSV2 injection, the percentage of Tregs in the spleen was increased after three DDP treatments (3.61% ± 0.12%; *p = 0.0185) relative to that in the mock group (2.40% ± 0.14%) but was decreased after three oHSV2 treatments (1.36% ± 0.08%; *p = 0.0180) (Figure 4B). In addition, the percentage of MDSCs in the spleen was significantly decreased in both the oHSV2 (1.85% ± 0.08%; ***p = 0.0005) and DDP (1.97% ± 0.09%; ***p = 0.0007) treatment groups compared with the mock group (3.98% ± 0.08%) (Figure 4C). NK cells are a subset of lymphocytes that mainly participate in innate immunity and play a key role in antitumor immune responses. The percentage of NK cells in the mock group was 7.75% ± 0.53%, higher than that in the DDP group (4.65% ± 0.27%; *p = 0.0389) and lower than that in the oHSV2 group (12.29% ± 0.32%; *p = 0.0131) (Figure 4D). The percentage of $CD8^+$ T cells in the spleen was

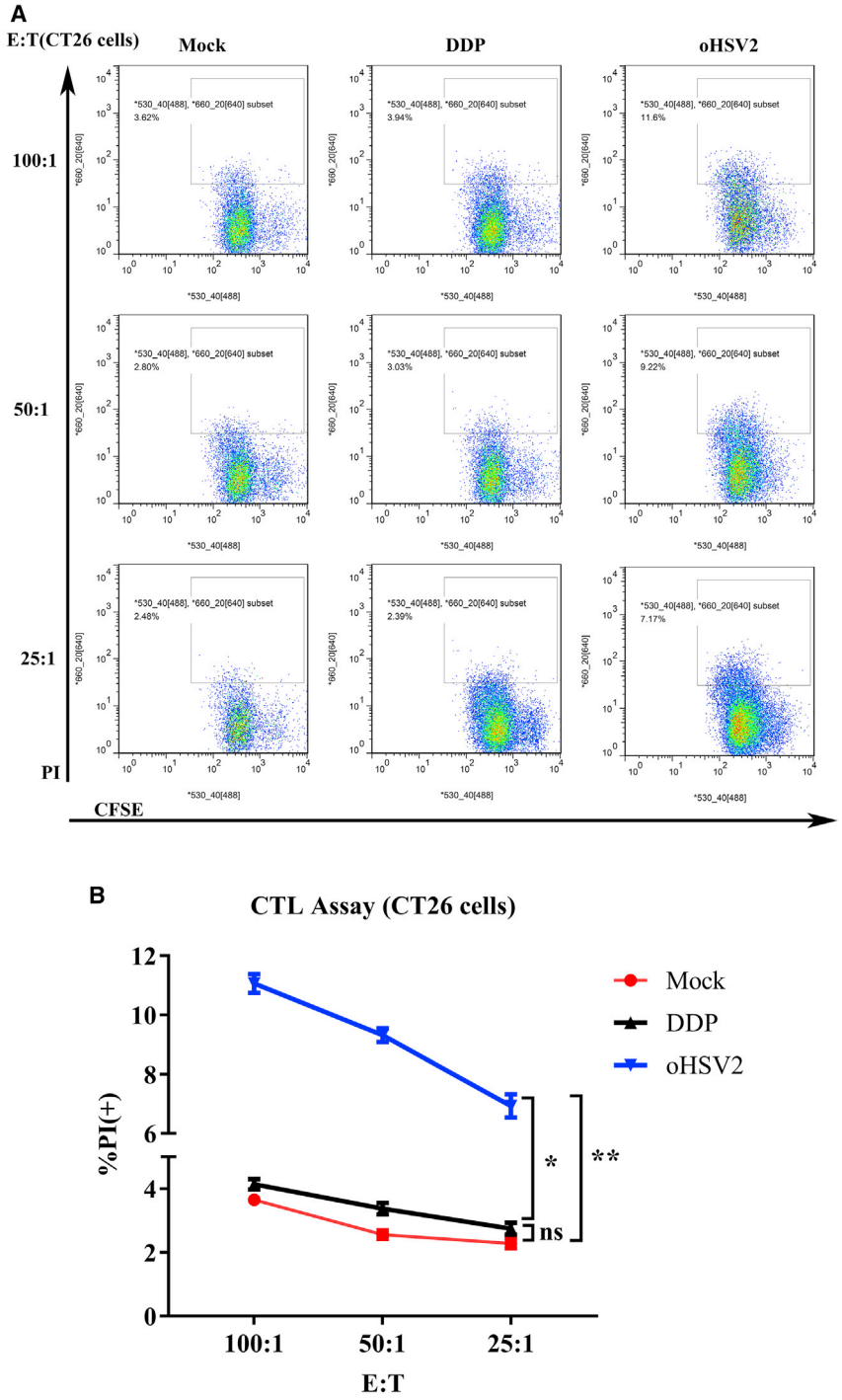

Figure 3. CTL Assay

Splenocytes harvested from three groups were cultured *in vitro* with CT26 cells at different E:T ratios. (A) Flow cytometric analysis results of one representative sample from each group at different E:T ratios. (B) Lymphocytes from the oHSV2 group led to increased PI expression in CFSE-labeled CT26 target cells after coincubation. The data are averages from three mice per treatment group. An unpaired Student's t test was used to analyze the significance of the difference between the groups. E:T, effector cell/target cell.

significantly increased after treatment with DDP (17.10% ± 0.53%; **p = 0.0013) and oHSV2 (12.7% ± 0.35%; **p = 0.0053) compared with that in the mock group (7.16% ± 0.46%) (Figure 4E). DCs are considered the most potent professional APCs *in vivo* and are the bridges that link innate and adaptive immunity. The percentage of DCs in the spleen was significantly decreased in the DDP group (2.78% ± 0.25%; **p = 0.0044); in contrast, the percentage of DCs in the oHSV2 group was significantly increased (8.24% ± 0.10%; **p = 0.0026) compared with that in the mock group (5.89% ± 0.18%) (Figure 4F). The development of memory T cells is often thought to be a characteristic of successful immune response to foreign antigens that mediate strong immunity. Indeed, $CD4^+$ T and $CD8^+$ memory T cells were detected. The percentages of $CD8^+$ memory T cells in the oHSV2 group (16.40% ± 0.65%; ***p = 0.0002) and the DDP group (12.33% ± 0.63%; **p = 0.0019) were significantly increased compared with those in the mock group (7.51% ± 0.19%) (Figure 4G). The percentages of $CD4^+$ memory T cells in the oHSV2 group (21.60% ± 0.50%; **p = 0.0011) and DDP group (23.97% ± 1.2%; **p = 0.0029) were significantly increased compared with the percentage in the mock group (15.00% ± 0.61%) (Figure 4H). These results suggest that treatment with oHSV2 reduced the level of immunosuppressive cells, including MDSCs and Tregs, and simultaneously enhanced T cell-dependent antitumor immunity. After DDP treatment, the percentage of $CD8^+$ T cells in the spleen was significantly higher but the percentage of DCs was significantly lower than that in the mock group, indicating that $CD8^+$ T cells remained in a relatively dormant state in the DDP group.

Virotherapy Has Similar Effects on the Bilateral TME

After observing the changes in splenic immune cells by flow cytometry, we further observed the immune status of the local TME. On the 12th day after treatment, the tumor volumes in the mock group and the chemotherapy group continuously increased. Most tumors in the mock group had already broken through the skin surface, while the tumors in the oHSV2 group tended to shrink, approaching their pretreatment size, and formed scabs.

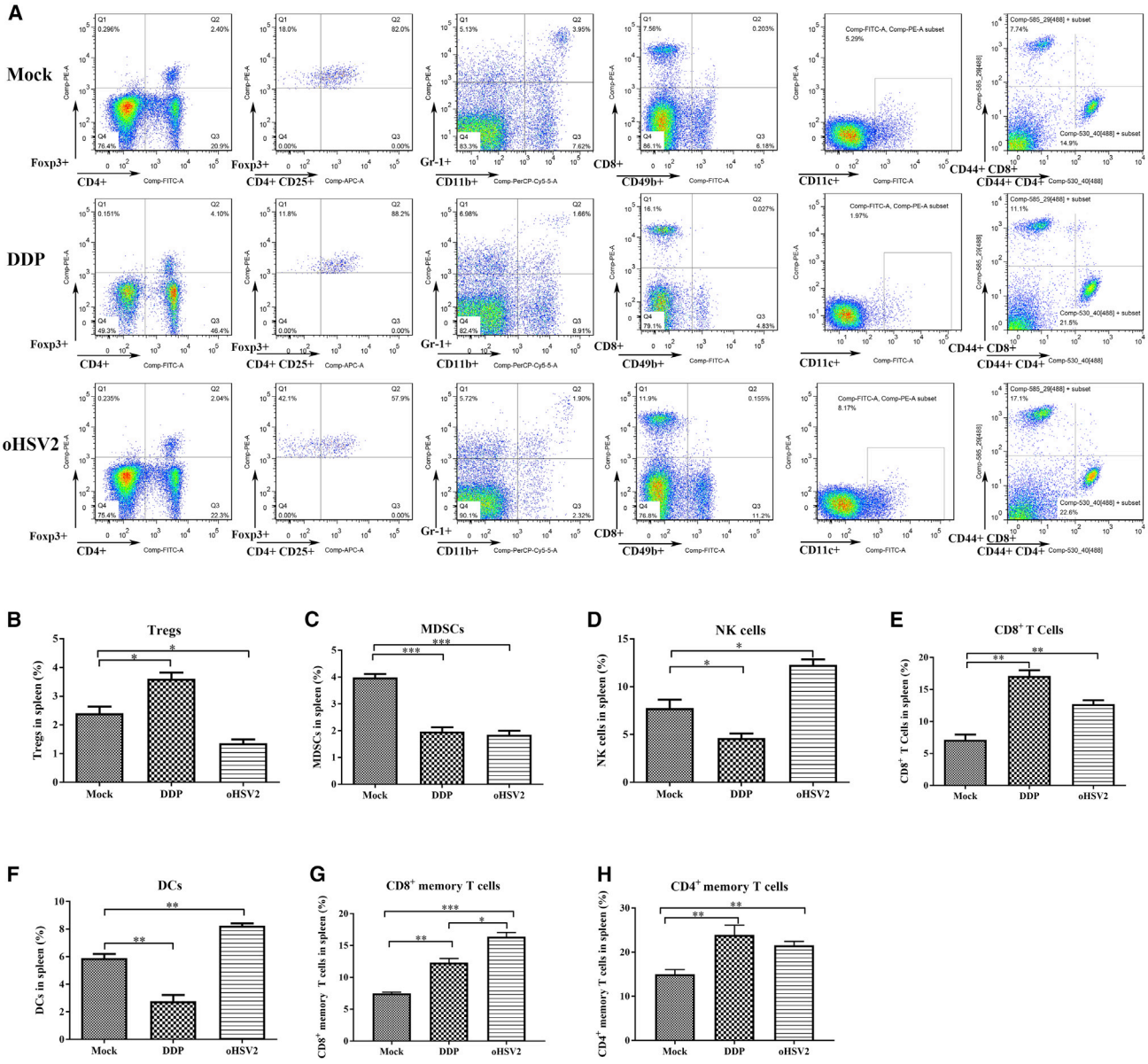

Figure 4. Percentages of Different Immune Cells in the Spleen, as Determined by Flow Cytometry

(A) Flow cytometric analysis of one representative sample from each treatment group. (B–H) The percentages of (B) Tregs (CD4, CD25, Foxp3); (C) MDSCs (Gr-1, CD11b); (D) NK cells (CD49b); (E) $CD8^+$ T cells; (F) DCs (CD11c); (G) $CD8^+$ memory T cells (CD44, CD8); and (H) $CD4^+$ memory T cells (CD44, CD4) were determined 2 days after the final treatment. An unpaired Student's t test was used to determine the significance between groups.

Bilateral tumor tissues and spleen tissues of mice in the three groups were sliced into pathological sections. Light microscopy of hematoxylin and eosin (H&E)-stained sections showed that tumor cells in the three groups exhibited different degrees of degeneration and necrosis (Figures 5B, 5E, 5H. and 5K). In the mock group, the tumor cells around the blood vessels remained healthy, but degeneration and necrosis occurred in tumor cells far from the blood vessels (Figure 5A). The boundaries of the degenerated cells were unclear, and the cytoplasm was lightly stained. The nuclei became pyknotic and then underwent karyorrhexis and karyolysis in some areas. In the DDP group, some tumor areas exhibited degeneration and necrosis. Many small blood vessels were seen in the area of degeneration, and no healthy tumor cells were seen surrounding the vessels (Figure 5D). In the oHSV2 group, tumor cells at the right-side inoculation site (the treated side) disappeared and were replaced by granulation and fibrotic scar tissue (Figure 5G). Microangiogenesis, fibroblast proliferation, inflammatory cells, and neutrophil infiltration were observed in this area (Figure 5I). Most tumor cells on the left side

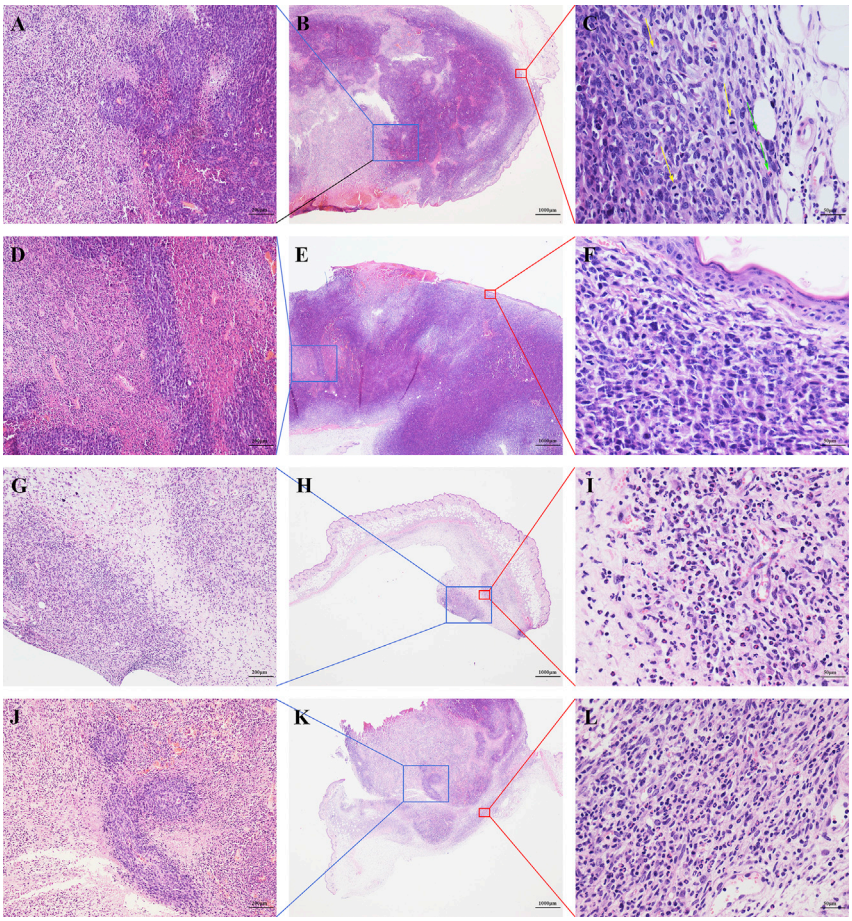

Figure 5. Histological Appearance of One Representative Tumor Sample from Each Treatment Group

H&E staining was used; n = 5 mice/group. (A–C) Mock group. (A) Tumor cells far from small blood vessels underwent degeneration and necrosis. Original magnification, ×100. (B) The area of degeneration and necrosis is at the center of the tumor. The skin exhibits ulcerations. Original magnification, ×20. (C) Dense tumor tissue with mitotic figures (yellow arrows). Minor infiltration of neutrophils (green arrows) is shown. Original magnification, ×400. (D–F) DDP group. (D) Area of tumor cell degeneration. Original magnification, ×100. (E) Skin ulcerations. Original magnification, ×20. (F) Minimal infiltration of lymphocytes and neutrophils is present. Original magnification, ×400. (G–I) oHSV2 group (oHSV2 injected/right-side tumor). (G) No definite tumor tissue is visible. Original magnification, ×100. (H) No clear tumor tissue is visible. The skin tissue is intact. Original magnification, ×20. (I) Small blood vessels. Fibroblast proliferation and inflammatory cell infiltration are shown. Neutrophils are readily visible. Original magnification, ×400. (J–L) oHSV2 group (oHSV2 uninjected/left-side tumor). (J) Island of tumor cells remaining in the degenerated area. Original magnification, ×100. (K) Most tumor cells underwent degeneration. Original magnification, ×20. (L) Small blood vessels. Fibroblast proliferation and inflammatory cell infiltration are shown. Neutrophils are readily visible. Original magnification, ×400.

(untreated side) were shrunken and necrotic. In some specimens, residual tumor cell islands surrounding small vessels were observed (Figure 5J). Fibroblasts proliferated, and acute inflammatory cells infiltrated into the area surrounding the tumor, forming a sheath-like structure (Figure 5L). These microscopic features showed that oHSV2 treatment induced a strong therapeutic response, which not only indicated a change in the tumor immune microenvironment but also provided a basis for the establishment of evaluation criteria for the therapeutic response.

An anti-Ki67 antibody was used to stain tumor tissues. The staining results revealed that the index of proliferating tumor cells in the mock and chemotherapy groups was significantly higher than that in the virotherapy group (Figure 6A). Interestingly, the Ki67 index in the spleen exhibited the opposite pattern—the virotherapy group had a much higher index than did the chemotherapy group (Figure 6A).

Subsequently, immunohistochemical (IHC) staining of tumor tissue was performed to investigate the distribution of immune cells in the TME. $CD8^+$ T cells, NK cells, and DCs were labeled. As shown in Figure 6B, the virotherapy group exhibited increased levels of these cells in bilateral tumors compared with the mock and chemotherapy groups (****$p < 0.0001$).

Therefore, treatment with oHSV2 significantly inhibited the growth and proliferation of tumor cells and, moreover, altered the tumor immune microenvironment. Remarkably, this effect was observed not only locally but also in distal tumor tissue.

Differential Expression of Immune Signatures in Bilateral Tumors

To further explore the effects of different therapeutic methods on the mouse immune status, RNA sequencing was applied to analyze the expression status of immune-related genes in the local TME, which reflects the immune response status.

Thirty samples, including bilateral tumors, were obtained from a total of 15 mice and divided without cluster analysis into three groups: the mock group (mock), the chemotherapy group (DDP), and the virotherapy group (oHSV2). Immune-related genes were divided into five categories according to their Gene Ontology (GO) annotation: innate immune-related genes (I, 225), adaptive immune-related genes (A, 112), humoral immune-related genes (H, 57), inflammation-related genes (IF, 152), and general immune response-related genes (G, 411). Detailed information on these genes is summarized in Data S1, and the percentage of genes in each category is shown in Figure 7B (Immune Gene Panel).

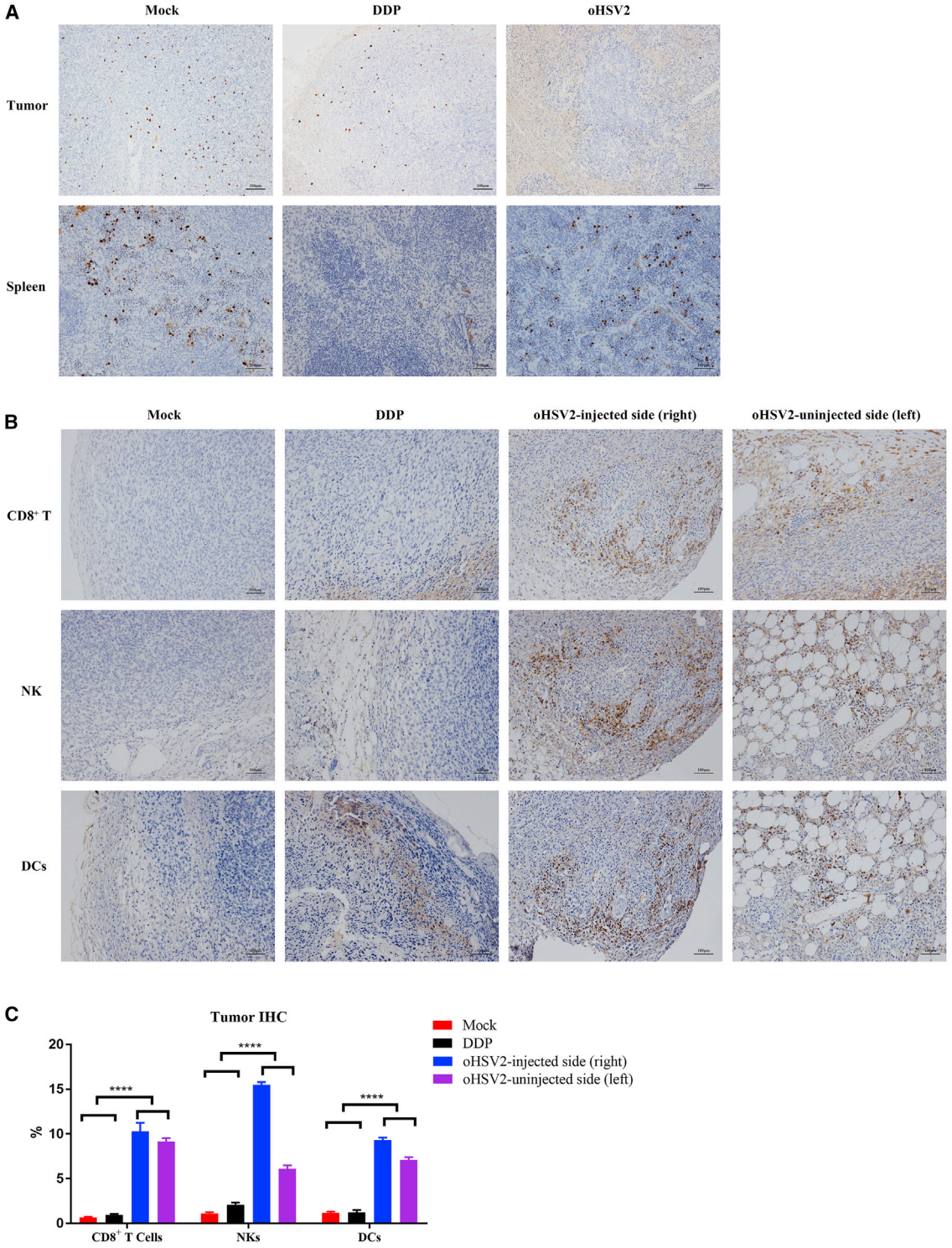

Figure 6. IHC Appearance of One Representative Sample from Each Treatment Group

(A) Ki67 expression in tumor tissue and spleen tissue. n = 5 samples/group; a representative sample from each group is shown. The three columns, from left to right, represent the mock group, the DDP group, and the virus group. Top row: tumor tissues (original magnification, ×100). Bottom row: spleen tissues (original

(legend continued on next page)

Immune signatures derived from a panel of 681 immune-related genes were extracted from the mRNA expression data of bilateral tumor tissues. The genes were clustered into different categories. Their expression levels are shown in Figure 7A, and the genes exhibited diverse expression patterns across the three groups. The RNA sequence expression patterns in the mock and chemotherapy groups were similar but significantly different from the pattern in the oHSV2 group. The RNA sequence expression patterns slightly differed between the bilateral tumors in the oHSV2 treatment group. Therefore, we speculate that the right-side tumor experienced a double hit (direct tumor cell killing and immune-induced tumor killing) after virotherapy and that the volume of the left-side tumor was reduced only by immune-induced tumor killing (Figure 7A). Next, differentially expressed genes were selected and defined by an adjusted p value of less than 0.01 with a $\log_2$ fold change of greater than 1 according the DESeq2 method.[15] The bilateral tumors were analyzed separately. Compared to mock treatment, DDP treatment induced upregulation of four immune-related genes and downregulation of two genes in the right-side tumor. However, oHSV2 treatment induced upregulation of 364 genes and downregulation of 43 genes. In the left-side tumors, only minimal expression differences were found between the DDP treatment group and the mock group; only two genes were downregulated in the DDP treatment group. In the oHSV2 treatment group, 254 genes were upregulated and 2 genes were downregulated relative to their levels in the mock treatment group (Figure 7B). As shown in the percentage stacked bar chart (Figure 7B), viral treatment not only significantly affected the local immune microenvironment of the right-side (treated side) tumor but also impacted the immune microenvironment of the left-side (untreated side) tumor. Compared with the baseline values (Immune Gene Panel and Immune-Related Genes), the percentage of adaptive, humoral, and inflammation-related genes among the upregulated genes was increased, and most of the downregulated genes were general immune response-related genes.

Gene Set Variation Analysis (GSVA) Expression Levels Scores in Bilateral Tumors

We then analyzed the differentially activated gene sets related to the immune response, cell proliferation, and multiple cell types between the left-side and right-side tumors in the three treatment groups using GSVA, a method for assessing the enrichment of gene sets in individual samples.[16]

GSVA revealed that the GSVA expression level scores of the bilateral tumors in the mock and chemotherapy groups were similar, but they were markedly different relative to those in the virotherapy group (Figure 7C). We focused on the virotherapy group and found that the differences in the TME of the right-side tumors were reasonable. We then focused on the TME of the left-side tumors and found that the cytotoxicity, tumoricidal effect, adhesion, and migration ability of immune cells in the virotherapy group were stronger than those in the other two groups. Additionally, the presentation of cancer antigens and the activation of T cells in the TME of the oHSV2-treated group were significantly stronger than those in the other two groups. In addition, some pathways, including IFN signaling, costimulatory signaling, cytokine and chemokine signaling, tumor necrosis factor (TNF) superfamily receptors, and autophagy, also exhibited differential expression. The above results indicated that mouse antitumor immunity was activated after virotherapy. The low levels of cell proliferation and antigen release in the right-side tumors were due to the small tumor size at the time of lesion collection, as observed in the previously examined pathological sections. The above conclusions prove that virotherapy can reshape the immune status of the local and distal TME and generate immune memory. Disruption of the inhibitory tumor immune microenvironment provides a solid foundation for immune cell function.

DISCUSSION

Oncolytic virotherapy, a promising candidate therapy, provides a new approach to improve the OS of cancer patients. Genetically engineered viruses can selectively infect and directly lyse tumor cells. Additionally, this process produces an immune response to not only viral antigens but also to tumor cell antigens, enabling the virus to induce a lasting immune response while eliminating existing tumors, thus counteracting metastatic and recurrent tumors.[17] From 2015 to 2016, talimogene laherparepvec (T-VEC, a modified HSV-1) was gradually approved for the treatment of advanced melanoma in the United States, Europe, and Australia.[18,19] The research and application of OV immunotherapy has progressed substantially, revealing more possibilities as well as challenges.

In this study, we selected DDP, a traditional chemotherapeutic drug, as the positive control to determine the comparative efficacy of oHSV2. CT26 cells were treated with oHSV2 at different MOIs and with DDP at different concentrations, and both treatments showed time- and dose-dependent responses. Although both treatments can reduce cell activity, the mechanisms are completely different. DDP exhibits broad-spectrum antitumor activity and mainly crosslinks cellular DNA, thus abolishing the function of DNA and inhibiting mitosis, leading to apoptosis.[20] As the killing effect of DDP is not specific to tumors, it can also cause a decrease in the leukocyte count. oHSV2 can strongly induce direct lysis and necrosis of tumor cells. Necrosis can induce an inflammatory response that can further improve the antitumor effect.[21] Therefore, compared with DDP, oHSV2 not only kills tumors directly but also can further stimulate the antitumor immune response to enhance the tumoricidal ability.

magnification, ×200). (B) IHC staining (original magnification, ×200). n = 5 samples/group; a representative sample from each group is shown. The expression in bilateral tumors in the mock and DDP treatment groups was similar; only one side is shown here. The infiltration rates of $CD8^+$ T cells, NK cells, and DCs in the bilateral tumors in the virus group were higher than those in the mock group and the chemotherapy group. (C) IHC quantification results. n = 5 samples/group. The IHC staining was scored with ImageJ software.

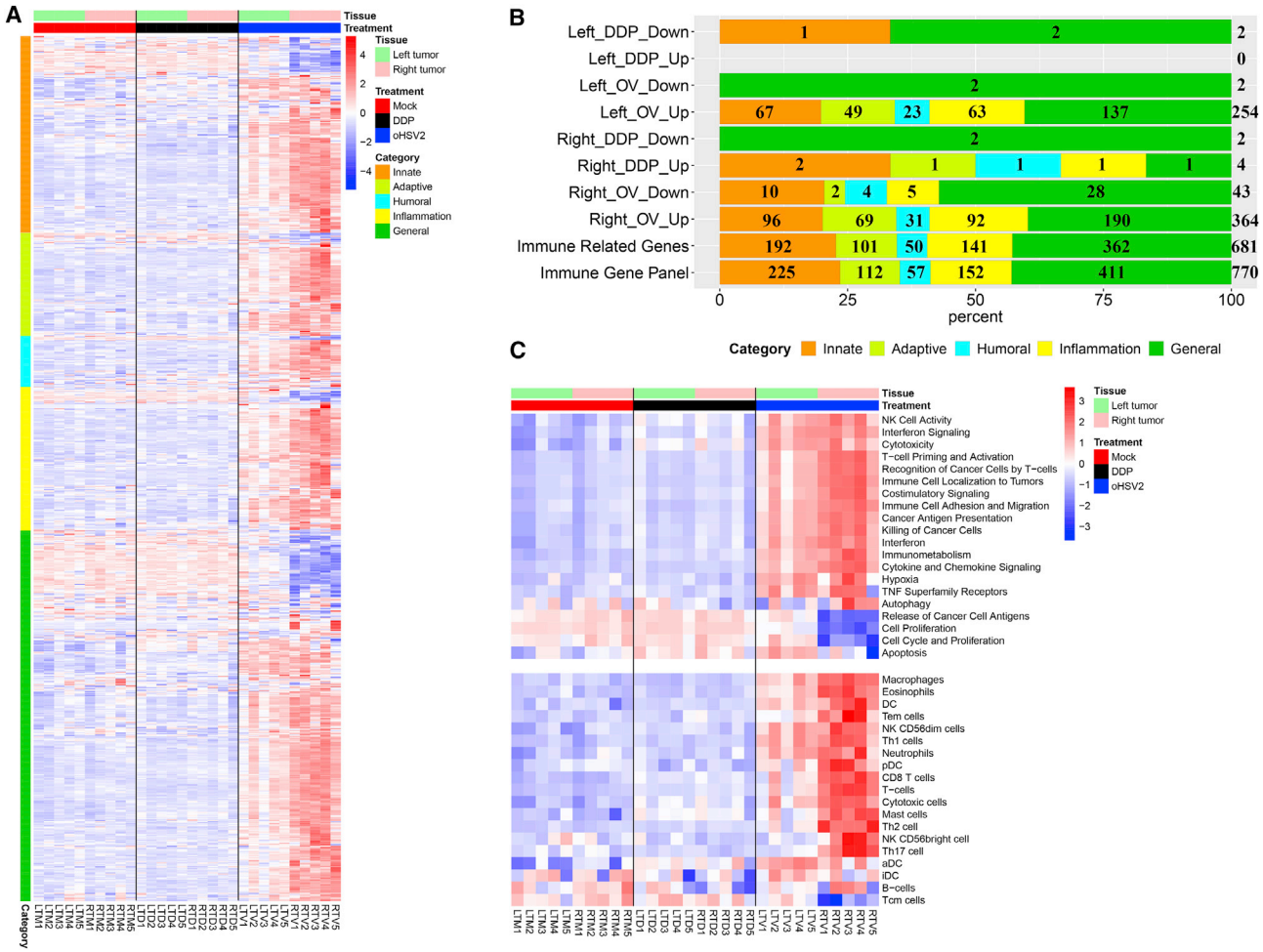

Figure 7. Differentially Expressed Immune Signatures in Bilateral Tumors

(A) The heatmap shows the expression of immune signatures containing 681 immune-related genes in bilateral tumors. Generally, these genes were classified into five categories: innate, adaptive, humoral, inflammation, and general immune response genes, with cluster analysis in each category. (B) Distribution of the differentially expressed immune-related gene categories. Immune-related mouse genes were divided into five categories according to the GO annotation. Immune Gene Panel: A total of 770 immune-related mouse genes were extracted from the nCounter Mouse PanCancer Immune Profiling Panel (NanoString). Immune-Related Genes: A total of 681 immune-related genes were extracted from the mRNA expression data from bilateral tumor tissues. Left_DDP_Down: Compared with mock treatment, DDP treatment induced downregulation of two genes, one belonging to the innate category and the other belonging to both the innate and general categories. (The meanings of the remaining terms are similar.) (C) GSVA of differentially activated gene sets. Each column represents the sample indicated at the bottom, and each row represents a gene set (see the complete set in Data S1). The GSVA expression level scores are depicted according to the color scale. Red and blue indicate expression levels above and below the median, respectively. The magnitude of deviation from the median is indicated by the color saturation. The upper panel shows immune response categories and cell proliferation-related gene sets, and the lower panel shows multiple cell types.

In recent decades, many studies have indicated that the anticancer action of all OVs is based on cancer cell lysis/necrosis caused by OV replication and on the antitumor immune response triggered by the lysed cells. The OV-induced antitumor immune response plays a more important role than OV-induced cell lysis in maintaining a long-term antitumor effect.[22] As our data showed, compared with DDP, oHSV2 exhibited an enhanced antitumor effect, significantly extended the mouse survival period, and improved the specific CTL response. Consistent with previous works, our established rechallenge and bilateral tumor-bearing models showed that oHSV2 caused a systemic long-term antitumor immune response while exerting a direct antitumor effect.[23] This tumor-specific immune response effectively inhibited both secondary identical tumorigenesis and the growth of distant nontreated tumors.

MDSCs are a heterogeneous population of cells with a marked ability to suppress T cell responses[24] and are considered an indicator of poor prognosis in some cancers.[25,26] Tregs are a subpopulation of suppressor T cells that generally suppress or downregulate the induction and proliferation of effector T cells.[27] OVs can effectively

reduce the levels of MDSCs and Tregs, thereby counteracting their suppressive activity on T cell proliferation via multiple mechanisms.[28–30] In our study, as expected, the levels of immunosuppressive cells (MDSCs and Tregs) in the mouse spleen decreased after oHSV2 treatment, and the levels of NK cells, $CD8^+$ T cells, and DCs, which play important roles in tumor killing, significantly increased. oHSV2 can effectively reduce the levels of MDSCs and Tregs in the spleen, thus effectively converting the immunosuppressive state. Collectively, these findings indicated that treatment with oHSV2 mobilized systemic antitumor immunity in mice.

The TME plays a key role in tumor genesis, invasion, and metastasis. Further studies on the TME will be helpful in revealing the mechanism of drug resistance and recurrence. Approaches that break the immunosuppressive state of the TME represent a breakthrough in combating drug resistance. Accumulating studies have shown that OVs can significantly alter the immune structure of the TME.[31] In addition, previous studies have shown that vesicular stomatitis virus (vsv-p14) increases the number of activated $CD4^+$ and $CD8^+$ T cells, NK cells, and natural killer T (NKT) cells in the spleen and increases the numbers of activated $CD4^+$ and $CD8^+$ cells in the TME (the overall number of CD4 cells was decreased).[32] Farrell et al.[33] showed that combination treatment with oHSV1 and immature myeloid DCs (iDCs) reduces the volume of established murine tumors and prolongs survival via the enhancement of antitumor immunity. Therefore, treatment with OVs alone or in combination with various immunomodulators enhances antitumor activity. In our study, oHSV2 treatment resulted in obvious degeneration and necrosis and a marked decrease in the proliferative activity of tumor cells; in addition, it promoted the immune response—mainly the inflammatory response and adaptive and humoral immunity—in the TME. Infiltration of neutrophils, NK cells, $CD8^+$ cells, and DCs into the connective tissue around the tumor was greater in the oHSV2 group than in the other two groups. Infiltration of these immune cells can effectively alter the immunosuppressive state of the TME and steer the TME toward an antitumor immune state, thus converting a cold tumor into a "hot" tumor.

The GSVA results revealed that virotherapy significantly altered the structure of immune cells in the bilateral TME. The bilateral TME exhibits a state of immune activation and generates immune memory. A study of adenoviruses indicated that autophagy regulates the processing of adenoviral proteins for antigen presentation. Specifically, upregulation of autophagy increased the presentation of virally delivered TAAs at the cell surface to enhance the antitumor immune response.[34] Numerous studies have indicated that type 1 IFNs can produce an antitumor response. In addition to their antiviral and antitumor properties, they stimulate various immune cell subtypes within the TME, including the cytotoxic activity of NK and $CD8^+$ T cells, the secretion of proinflammatory cytokines by macrophages, and the cross-presentation activity of mature DCs.[35] Another study demonstrated that attenuated measles virus (MV) can increase the IFN-dependent expression of TNF-related apoptosis-inducing ligand (TRAIL) on the surface of DCs, thereby inducing the cytotoxicity of myeloid $CD11c^+$ DCs and plasmacytoid DCs (pDCs), which may participate in the antitumor immune response.[36] Furthermore, several cytokines, such as IFN and TNF, can prolong neutrophil survival.[37] Because the interaction between OVs and immune cells is very complex, we intend to use informatics analysis approaches to screen the cytotoxic T cells that target TAAs released by virus-lysed tumor cells. We may also further target screened TAAs by genetically modifying OVs.

In summary, our results suggest that oHSV2 can effectively eliminate primary tumors and generate tumor-specific immunity to inhibit tumor recurrence and metastasis. Additionally, in mice, treatment with this virus altered the immune status in the spleen and nontreated tumors, leading to increased effectiveness of tumor treatment. Treatment with oHSV2 transforms an inhibitory tumor immune microenvironment into an inflammatory microenvironment that benefits antitumor activity. The increases in neutrophils, DCs, and B cells enhance the presentation of TAAs and further induce specific T cell responses. In addition, recent studies have shown that tumor neoantigens are key targets for many therapies.[38] Tumor neoantigens are released during tumor cell lysis and death, and this process might be worth exploring. Indeed, many approaches can be used to develop the activity of OVs against tumors. For example, arming viruses with immunostimulatory molecules would allow them to more effectively stimulate the immune system to produce long-term antitumor effects;[39,40] combining these viruses with traditional and novel approaches is a new research trend.[41,42] Cancer virotherapy has broad application prospects. However, improving the regulation of the balance between antitumor and antiviral activities remains challenging and requires further exploration.

MATERIALS AND METHODS

Mice and Cells

Six-week-old female BALB/c, CB-17 SCID, and SCID-beige mice (Beijing Vital River Laboratory Animal Technology Co., Ltd.) were maintained under specific pathogen-free conditions. Mice were treated according to the National Institutes of Health guidelines. The protocol was approved by the Committee on the Ethics of Animal Experiments of the National Cancer Center/Cancer Hospital, Chinese Academy of Medical Sciences (CAMS), and Peking Union Medical College.

The mouse colon cancer cell line CT26.WT and mouse breast cancer cell line 4T1, derived from BALB/c mice, were purchased from the National Infrastructure of Cell Line Resource (Beijing, China) and were cultured in RPMI 1640 medium (without HEPES [*N*-2-hydroxyethylpiperazine-*N*′-2-ethanesulfonic acid]) supplemented with 10% fetal bovine serum (FBS) and DMEM/F12 medium supplemented with 10% FBS, respectively. Cells were incubated at 37°C in a humidified atmosphere containing 5% CO_2.

Virus and Drugs

OV oHSV2 was provided by Wuhan Binhui Biotechnology Co., Ltd. (Wuhan, China). The virus was an attenuated oHSV2 derived from

the wild-type HSV-2 strain HG52. The specific construction method has been described previously.[14]

DDP was purchased from Qilu Pharmaceutical Co., Ltd. and diluted to 2 mg/mL in phosphate-buffered saline (PBS) before use.

Cell Proliferation Assays

Cell proliferation was assessed with a CCK-8 assay (Dojindo, Japan). CT26 cells were seeded in a 96-well plate at a density of 5,000 cells/well. The wells containing seeded cells were divided into several sets, and each set was run in triplicate. These CT26 cells were incubated with oHSV2 at different MOIs and DDP at different concentrations. After incubation for the indicated times (24, 48, and 72 h), the culture medium was removed, and 100 μL of a mixture containing 10% CCK-8 reagent was added in the dark. After incubation for an additional 1 h at 37°C in a humidified atmosphere containing 5% CO_2, the plates were read in a model 550 microplate reader (Bio-Rad, Japan) at 450 nm with a correction value of 655 nm.

Animal Model Establishment and Treatments

To explore the therapeutic effect of oHSV2 and DDP, we established an animal model using CT26 cells grown in female BALB/c mice. CT26 cells (3×10^5) were inoculated s.c. on the right side of the dorsal area of immunocompetent female BALB/C female mice. Approximately 5 days after tumor inoculation, when the tumors were palpable, the mice were separated into three groups (mock, oHSV2, and DDP) with an even distribution of tumor volumes (n = 5–8/group). The groups were treated as follows: (1) DDP (6 mg/kg) alone was injected intraperitoneally (i.p.) every 2 days for a total of three injections; (2) oHSV2 (2×10^6 plaque-forming units [PFU]) alone; or (3) RPMI 1640 SFM (100 μL) as a mock agent were injected intratumorally (i.t.) every other day for a total of three injections (Figure 2A). The tumor diameters and body weights were measured every other day. The survival of mice in every group was monitored during the experimental period.

We then performed a rechallenge experiment. Fifteen days after the first treatment, 12 mice per group (mock and oHSV2) were inoculated with another tumor on the contralateral side (left) of the dorsal area. Six mice were reinjected with CT26 cells (3×10^5), and the other six were reinjected with 4T1 cells (5×10^4). The tumor size was measured every other day. When the volume of the tumor on either side reached 2,500 mm^3, the mouse was considered dead.

A similar animal model was established by s.c. bilateral (two tumor nodules were generated) inoculation of immunocompetent female BALB/c mice and immunodeficient female CB-17 SCID and SCID-beige mice. Mice were treated unilaterally (right side only) with oHSV2 (2×10^6 PFU) alone, DDP alone, or RPMI 1640 SFM (100 μL); the other nodule was left untreated. Only tumor growth was followed over time.

Each group contained five to eight mice, and the experiments were repeated at least three times with similar results. In the experiments, tumor volumes were measured every 2 days following treatments and were calculated with the following formula: volume = (length × width2)/2. Mice were sacrificed by cervical dislocation when tumor volumes reached 2,500 mm^3 or when they showed distress to avoid unnecessary suffering. The weights of the mice were measured every 2 days following treatments.

CTL Assay

To determine whether oHSV2 induced a tumor-specific CTL response, CTL experiments were conducted. The spleens were surgically removed 2 days after the final treatment. Splenic lymphocytes were isolated by gradient centrifugation using lymphocyte separation medium (DKW33-R0100, Dakewe Biotech, Shenzhen, China) at room temperature and washed twice with PBS. CT26 cells and 4T1 cells, as target cells, were labeled with 0.5 mmol/L carboxyfluorescein succinimidyl ester (CFSE) for 8 min at 37°C. The labeling reaction was terminated with complete medium for 8 min at 0°C. After centrifugation, the cell concentration was adjusted to 4×10^5 cells/mL. Then, lymphocyte effector cells and target cells were mixed at E:T ratios of 100:1, 50:1, and 25:1. After incubation at 37°C and 5% CO_2 for 4 h, cells were harvested and labeled with 1 mg/mL PI for 5 min at room temperature, subjected to flow cytometry (BD LSR II) and analyzed using FlowJo and GraphPad Prism 7 software.

Isolation and Flow Cytometric Analysis of Splenic Immune Cells

Two days after the final treatment mentioned above, mice (3 mice/group) were sacrificed by cervical dislocation for characterization of the immune cells (Tregs, $CD8^+$ T cells, NK cells, MDSCs, and DCs) in the spleen. Memory T cells were detected on day 15. Splenic lymphocytes were harvested as described above. For surface labeling, cells were suspended in staining buffer and incubated for 15 min at room temperature in the dark with the following fluorophore-conjugated anti-mouse monoclonal antibodies (mAbs) (BioLegend): fluorescein isothiocyanate (FITC)-conjugated anti-CD4, allophycocyanin (APC)-conjugated anti-CD25, phycoerythrin (PE)-conjugated anti-CD8, FITC-conjugated anti-CD49b, PE-Cy5-conjugated anti-CD11b, PE-conjugated anti-Gr-1, FITC-conjugated anti-CD11c, and APC-conjugated anti-CD44. For intracellular FOXP3 staining, cells were fixed and permeabilized according to the manufacturer's protocol and incubated with a PE-conjugated anti-FOXP3 antibody for 30 min at room temperature in the dark. The pellet was finally resuspended in 300 μL of PBS, subjected to flow cytometry (BD LSR II), and analyzed using FlowJo and GraphPad Prism 7 software.

Histology and IHC Staining

For histological evaluation, bilateral tumors and spleen tissues were dissected from 15 mice and were formalin fixed and paraffin embedded (FFPE) on day 12 after the first treatment. Four-micrometer-thick tissue sections were prepared and stained with H&E. The same tissue sections were used for IHC staining. IHC experiments were carried out according to a standard protocol. Briefly, after deparaffinization in xylene and hydration in graded concentrations of ethanol, 3% hydrogen peroxide was applied to block endogenous

peroxide activity. Then, sections were boiled in 0.01 M citrate buffer (pH 6.0) for 10 min in a microwave oven. After cooling at room temperature, sections were incubated with normal goat serum to reduce nonspecific binding. Sections were then incubated with the primary antibody at 4°C overnight. Next, appropriate horseradish peroxidase (HRP)-conjugated secondary antibodies were used to detect the primary antibodies, and immunoreactions were visualized with the 3,3′-diaminobenzidine (DAB) chromogen. Sections were counterstained with hematoxylin and dehydrated in ethanol and xylene.

The following antibodies were used for the IHC experiment: anti-Ki67 (SP6) (ab16667), anti-mouse CD8a (53-6.7) (eBioscience, 14-0081-85), anti-mouse CD11c mAb (N418) (eBioscience, 14-0114-81), and anti-mouse CD49b (DX5) (STEMCELL, 60020). Staining was observed using a microscope (a Nikon Eclipse 80i was used for microscopic observation, and the sections on the slides were imaged with Nikon Digital Sight DS-Ri1).

RNA Preparation

Pieces of the bilateral tumors were submerged in 5 vol of RNAlater (Invitrogen) (n = 5 samples/group). Total RNA was isolated from these tissues using TRIzol (Life Technologies). The RNA concentrations in the samples were measured using a NanoDrop 2000 instrument (Thermo Fisher Scientific) and checked for quality on formaldehyde agarose gels. All RNA samples used in this study exhibited optical density $(OD)_{260/280}$ ratios greater than 1.9 and RNA integrity numbers (RINs) greater than 8.5.

Bioinformatics Analysis

Differential expression analyses of mRNA expression data in 30 samples were performed by using the DESeq2 R package v1.20.0. A total of 770 immunology-related mouse genes, created from the nCounter Mouse PanCancer Immune Profiling Panel (NanoString), were then implemented as candidate genes in this study; detailed annotations for these genes are listed in Data S1. GSVA was employed to detect the variation values of the GO term pathways in each group using the R package GSVA. The gene list is shown in Data S2.

Statistical Analysis

All experiments were repeated in triplicate unless otherwise stated. Statistical analyses were performed using GraphPad Prism software version 7 (GraphPad Software), and statistical significance was defined as $p < 0.05$. Flow cytometry data were compared using a two-tailed, unpaired Student's t test. Two-way analysis of variance (ANOVA) was performed on the experimental data for tumor volumes and mouse weights. The Kaplan-Meier method with the log-rank test was used to compare survival curves; survival was defined as the time from treatment until the endpoint was reached. The results are presented as the mean ± standard error of the mean (SEM).

Differentially expressed genes were compared with Student's t test, and adjusted p values of less than 0.01 and fold changes of greater than 2 were considered to indicate significant dysregulation. p values were adjusted by the Benjamini-Hochberg (BH) method. Adjusted p values are also called q values. Data were analyzed using R (version 3.5.1).

SUPPLEMENTAL INFORMATION

Supplemental Information can be found online at https://doi.org/10.1016/j.omto.2019.12.012.

AUTHOR CONTRIBUTIONS

X.H., W.Z., S.L., B.L., and K.Z. contributed to the study design and concept. X.H. and W.Z. contributed substantially to the acquisition, analysis, and interpretation of data in all experiments and were the primary authors of this manuscript. J.L. contributed to solving pathological problems. Y.Z., B.Z., and C.Z. contributed to the acquisition of data in animal experiments. L.F. contributed to guiding biological information analysis. K.Z., S.L., and B.L. supervised the study. All authors read and approved the final manuscript.

CONFLICTS OF INTEREST

The authors declare no competing interests.

ACKNOWLEDGMENTS

This work was supported by the CAMS Initiative for Innovative Medicine (2017-I2M-3-020) and the National Natural Science Foundation of China (81650016). We thank Prof. Binlei Liu (Hubei University of Technology) and Wuhan Binhui Biotechnology Co., Ltd. for the kind gift of the oHSV2.

REFERENCES

1. Bray, F., Ferlay, J., Soerjomataram, I., Siegel, R.L., Torre, L.A., and Jemal, A. (2018). Global cancer statistics 2018: GLOBOCAN estimates of incidence and mortality worldwide for 36 cancers in 185 countries. CA Cancer J. Clin. *68*, 394–424.

2. Siegel, R., Desantis, C., and Jemal, A. (2014). Colorectal cancer statistics, 2014. CA Cancer J. Clin. *64*, 104–117.

3. Pol, J.G., Lévesque, S., Workenhe, S.T., Gujar, S., Le Boeuf, F., Clements, D.R., Fahrner, J.E., Fend, L., Bell, J.C., Mossman, K.L., et al. (2018). Trial watch: oncolytic viro-immunotherapy of hematologic and solid tumors. Oncoimmunology *7*, e1503032.

4. Twumasi-Boateng, K., Pettigrew, J.L., Kwok, Y.Y.E., Bell, J.C., and Nelson, B.H. (2018). Oncolytic viruses as engineering platforms for combination immunotherapy. Nat. Rev. Cancer *18*, 419–432.

5. Raja, J., Ludwig, J.M., Gettinger, S.N., Schalper, K.A., and Kim, H.S. (2018). Oncolytic virus immunotherapy: future prospects for oncology. J. Immunother. Cancer *6*, 140.

6. Chon, H.J., Lee, W.S., Yang, H., Kong, S.J., Lee, N.K., Moon, E.S., Choi, J., Han, E.C., Kim, J.H., Ahn, J.B., et al. (2019). Tumor microenvironment remodeling by intratumoral oncolytic vaccinia virus enhances the efficacy of immune-checkpoint blockade. Clin. Cancer Res. *25*, 1612–1623.

7. Brown, M.C., Holl, E.K., Boczkowski, D., Dobrikova, E., Mosaheb, M., Chandramohan, V., Bigner, D.D., Gromeier, M., and Nair, S.K. (2017). Cancer immunotherapy with recombinant poliovirus induces IFN-dominant activation of dendritic cells and tumor antigen-specific CTLs. Sci. Transl. Med. *9*, eaan4220.

8. Delaunay, T., Violland, M., Boisgerault, N., Dutoit, S., Vignard, V., Münz, C., Gannage, M., Dréno, B., Vaivode, K., Pjanova, D., et al. (2017). Oncolytic viruses sensitize human tumor cells for NY-ESO-1 tumor antigen recognition by $CD4^+$ effector T cells. OncoImmunology *7*, e1407897.

9. van Vloten, J.P., Workenhe, S.T., Wootton, S.K., Mossman, K.L., and Bridle, B.W. (2018). Critical interactions between immunogenic cancer cell death, oncolytic viruses, and the immune system define the rational design of combination immunotherapies. J. Immunol. *200*, 450–458.

10. Kim, Y., Clements, D.R., Sterea, A.M., Jang, H.W., Gujar, S.A., and Lee, P.W. (2015). Dendritic cells in oncolytic virus-based anti-cancer therapy. Viruses *7*, 6506–6525.

11. Pol, J.G., Zhang, L., Bridle, B.W., Stephenson, K.B., Rességuier, J., Hanson, S., Chen, L., Kazdhan, N., Bramson, J.L., Stojdl, D.F., et al. (2014). Maraba virus as a potent oncolytic vaccine vector. Mol. Ther. *22*, 420–429.

12. Ribas, A., Dummer, R., Puzanov, I., VanderWalde, A., Andtbacka, R.H.I., Michielin, O., Olszanski, A.J., Malvehy, J., Cebon, J., Fernandez, E., et al. (2018). Oncolytic virotherapy promotes intratumoral T cell infiltration and improves anti-PD-1 immunotherapy. Cell *174*, 1031–1032.

13. Bridle, B.W., Nguyen, A., Salem, O., Zhang, L., Koshy, S., Clouthier, D., Chen, L., Pol, J., Swift, S.L., Bowdish, D.M., et al. (2016). Privileged antigen presentation in splenic B cell follicles maximizes T cell responses in prime-boost vaccination. J. Immunol. *196*, 4587–4595.

14. Zhao, Q., Zhang, W., Ning, Z., Zhuang, X., Lu, H., Liang, J., Li, J., Zhang, Y., Dong, Y., Zhang, Y., et al. (2014). A novel oncolytic herpes simplex virus type 2 has potent antitumor activity. PLoS ONE *9*, e93103.

15. Love, M.I., Huber, W., and Anders, S. (2014). Moderated estimation of fold change and dispersion for RNA-seq data with DESeq2. Genome Biol. *15*, 550.

16. Hänzelmann, S., Castelo, R., and Guinney, J. (2013). GSVA: gene set variation analysis for microarray and RNA-seq data. BMC Bioinformatics *14*, 7.

17. Howells, A., Marelli, G., Lemoine, N.R., and Wang, Y. (2017). Oncolytic viruses—interaction of virus and tumor cells in the battle to eliminate cancer. Front. Oncol. *7*, 195.

18. Coffin, R. (2016). Interview with Robert Coffin, inventor of T-VEC: the first oncolytic immunotherapy approved for the treatment of cancer. Immunotherapy *8*, 103–106.

19. Andtbacka, R.H., Kaufman, H.L., Collichio, F., Amatruda, T., Senzer, N., Chesney, J., Delman, K.A., Spitler, L.E., Puzanov, I., Agarwala, S.S., et al. (2015). Talimogene laherparepvec improves durable response rate in patients with advanced melanoma. J. Clin. Oncol. *33*, 2780–2788.

20. Dasari, S., and Tchounwou, P.B. (2014). Cisplatin in cancer therapy: molecular mechanisms of action. Eur. J. Pharmacol. *740*, 364–378.

21. Achard, C., Surendran, A., Wedge, M.E., Ungerechts, G., Bell, J., and Ilkow, C.S. (2018). Lighting a fire in the tumor microenvironment using oncolytic immunotherapy. EBioMedicine *31*, 17–24.

22. Speranza, M.C., Kasai, K., and Lawler, S.E. (2016). Preclinical mouse models for analysis of the therapeutic potential of engineered oncolytic herpes viruses. ILAR J. *57*, 63–72.

23. Hirvinen, M., Capasso, C., Guse, K., Garofalo, M., Vitale, A., Ahonen, M., Kuryk, L., Vähä-Koskela, M., Hemminki, A., Fortino, V., et al. (2016). Expression of DAI by an oncolytic vaccinia virus boosts the immunogenicity of the virus and enhances antitumor immunity. Mol. Ther. Oncolytics *3*, 16002.

24. Gabrilovich, D.I., and Nagaraj, S. (2009). Myeloid-derived suppressor cells as regulators of the immune system. Nat. Rev. Immunol. *9*, 162–174.

25. Wang, Z., Zhang, L., Wang, H., Xiong, S., Li, Y., Tao, Q., Xiao, W., Qin, H., Wang, Y., and Zhai, Z. (2015). Tumor-induced $CD14^{+}HLA\text{-}DR^{-/low}$ myeloid-derived suppressor cells correlate with tumor progression and outcome of therapy in multiple myeloma patients. Cancer Immunol. Immunother. *64*, 389–399.

26. Tian, T., Gu, X., Zhang, B., Liu, Y., Yuan, C., Shao, L., Guo, Y., and Fan, K. (2015). Increased circulating CD14(+)HLA-DR-/low myeloid-derived suppressor cells are associated with poor prognosis in patients with small-cell lung cancer. Cancer Biomark. *15*, 425–432.

27. Tanaka, A., and Sakaguchi, S. (2017). Regulatory T cells in cancer immunotherapy. Cell Res. *27*, 109–118.

28. Katayama, Y., Tachibana, M., Kurisu, N., Oya, Y., Terasawa, Y., Goda, H., Kobiyama, K., Ishii, K.J., Akira, S., Mizuguchi, H., and Sakurai, F. (2018). Oncolytic reovirus inhibits immunosuppressive activity of myeloid-derived suppressor cells in a TLR3-dependent manner. J. Immunol. *200*, 2987–2999.

29. Oh, E., Choi, I.K., Hong, J., and Yun, C.O. (2017). Oncolytic adenovirus coexpressing interleukin-12 and decorin overcomes Treg-mediated immunosuppression inducing potent antitumor effects in a weakly immunogenic tumor model. Oncotarget *8*, 4730–4746.

30. Esaki, S., Goshima, F., Kimura, H., Murakami, S., and Nishiyama, Y. (2013). Enhanced antitumoral activity of oncolytic herpes simplex virus with gemcitabine using colorectal tumor models. Int. J. Cancer *132*, 1592–1601.

31. Lichty, B.D., Breitbach, C.J., Stojdl, D.F., and Bell, J.C. (2014). Going viral with cancer immunotherapy. Nat. Rev. Cancer *14*, 559–567.

32. Le Boeuf, F., Gebremeskel, S., McMullen, N., He, H., Greenshields, A.L., Hoskin, D.W., Bell, J.C., Johnston, B., Pan, C., and Duncan, R. (2017). Reovirus FAST protein enhances vesicular stomatitis virus oncolytic virotherapy in primary and metastatic tumor models. Mol. Ther. Oncolytics *6*, 80–89.

33. Farrell, C.J., Zaupa, C., Barnard, Z., Maley, J., Martuza, R.L., Rabkin, S.D., and Curry, W.T., Jr. (2008). Combination immunotherapy for tumors via sequential intratumoral injections of oncolytic herpes simplex virus 1 and immature dendritic cells. Clin. Cancer Res. *14*, 7711–7716.

34. Klein, S.R., Jiang, H., Hossain, M.B., Fan, X., Gumin, J., Dong, A., Alonso, M.M., Gomez-Manzano, C., and Fueyo, J. (2016). Critical role of autophagy in the processing of adenovirus capsid-incorporated cancer-specific antigens. PLoS ONE *11*, e0153814.

35. Zitvogel, L., Galluzzi, L., Kepp, O., Smyth, M.J., and Kroemer, G. (2015). Type I interferons in anticancer immunity. Nat. Rev. Immunol. *15*, 405–414.

36. Achard, C., Guillerme, J.B., Bruni, D., Boisgerault, N., Combredet, C., Tangy, F., Jouvenet, N., Grégoire, M., and Fonteneau, J.F. (2016). Oncolytic measles virus induces tumor necrosis factor-related apoptosis-inducing ligand (TRAIL)-mediated cytotoxicity by human myeloid and plasmacytoid dendritic cells. OncoImmunology *6*, e1261240.

37. Colotta, F., Re, F., Polentarutti, N., Sozzani, S., and Mantovani, A. (1992). Modulation of granulocyte survival and programmed cell death by cytokines and bacterial products. Blood *80*, 2012–2020.

38. Hu, Z., Ott, P.A., and Wu, C.J. (2018). Towards personalized, tumour-specific, therapeutic vaccines for cancer. Nat. Rev. Immunol. *18*, 168–182.

39. Kemp, V., van den Wollenberg, D.J.M., Camps, M.G.M., van Hall, T., Kinderman, P., Pronk-van Montfoort, N., and Hoeben, R.C. (2019). Arming oncolytic reovirus with GM-CSF gene to enhance immunity. Cancer Gene Ther. *26*, 268–281.

40. Kowalsky, S.J., Liu, Z., Feist, M., Berkey, S.E., Ma, C., Ravindranathan, R., Dai, E., Roy, E.J., Guo, Z.S., and Bartlett, D.L. (2018). Superagonist IL-15-armed oncolytic virus elicits potent antitumor immunity and therapy that are enhanced with PD-1 blockade. Mol. Ther. *26*, 2476–2486.

41. Ajina, A., and Maher, J. (2017). Prospects for combined use of oncolytic viruses and CAR T-cells. J. Immunother. Cancer *5*, 90.

42. Jonas, B.A. (2017). Combination of an oncolytic virus with PD-L1 blockade keeps cancer in check. Sci. Transl. Med. *9*, eaan2781.